Materials Science in Semiconductor Processing 196 (2025) 109668

Contents lists available at ScienceDirect

Materials Science in Semiconductor Processing

journal homepage: www.elsevier.com/locate/mssp

A comprehensive statistical study of the post-programming conductance drift in HfO_2-based memristive devices

D. Maldonado [a,b], C. Acal [c], H. Ortiz [c], A.M. Aguilera [c], J.E. Ruiz-Castro [c], A. Cantudo [a], A. Baroni [d], K. Dorai Swamy Reddy [d], S. Pechmann [e], M. Uhlmann [d], C. Wenger [d,f], E. Pérez [d,f], J.B. Roldán [a,*]

[a] Departamento de Electrónica y Tecnología de Computadores, Universidad de Granada, Facultad de Ciencias, 18071, Granada, Spain
[b] Departamento de Informática y Estadística, Esc. Tec. Sup. de Ingeniería Informática, Universidad Rey Juan Carlos, Móstoles, 28933, Madrid, Spain
[c] Departamento de Estadística e Investigación Operativa e Instituto de Matemáticas (IMAG), Universidad de Granada, Facultad de Ciencias, Avd. Fuentenueva s/n, 18071, Granada, Spain
[d] IHP GmbH - Leibniz-Institut für innovative Mikroelektronik, 15236, Frankfurt (Oder), Germany
[e] Micro- and Nanosystems Technology, Technical University of Munich, Munich, Germany
[f] Brandenburgische Technische Universität (BTU) Cottbus-Senftenberg, 03046, Cottbus, Germany

ARTICLE INFO

Keywords:
Resistive switching memory
Distribution function
Conductance state drift
Multi-level
Memristive device

ABSTRACT

The conductance drift in HfO_2-based memristors is a critical reliability concern that impacts in their application in non-volatile memory and neuromorphic computing integrated circuits. In this work we present a comprehensive statistical analysis of the conductance drift behavior in resistive random access memories (RRAM) whose physics is based on valence change mechanisms. We experimentally characterize the conductance time evolution in six different resistance states and analyze the suitability of various probability distributions to model the observed variability. Our results reveal that the log-logistic probability distribution provides the best fit to the experimental data for the resistance multilevels and the measured post-programming times under consideration. Additionally, we employ an analysis of variance (ANOVA) to statistically analyze the post-programming time and current level effects on the observed variability. Finally, in the context of the Stanford compact model, we describe how variability has to be implemented to obtain the probability distribution of measured current values.

1. Introduction

RRAM, a subset of memristors, are under study by the Academy and the industry for their outstanding applications in state-of-the-art nanoelectronics [1]. Although there are other memristive technologies based on phase-change materials [2], magnetic materials [3], ferroelectric materials [4], etc., the maturity of RRAM technology makes it a key player in future integrated circuits. In relation to non-volatile memory circuits, RRAM allow successful industrial exploitation. For instance, in the 22 nm technology node different chips have been demonstrated by industry leaders like TSMC [5] and INTEL [6]. Other interesting fields of research and development are connected to high frequency switches [7] and advanced data encryption [8]. In addition, these devices, along with other types of memristive devices, show great potential in the neuromorphic computing landscape [9–13].

Resistive memories have promising features in the non-volatile memory context, such as an endurance above 10^{10} cycles, short writing/reading times (<10 ns), scalability down to ~2 nm, resilience to high radiation environments [14] and CMOS fabrication technology compatibility.

Most RRAM devices described in the literature fit two main categories: conductive bridge RAMs and valence change memories (VCMs) [15,16]. The devices we analyze here belong to the latter group. In particular, our devices show filamentary conduction that is connected to the formation and rupture of conductive filaments (CF) that produce a short circuit between the electrodes. CFs are zones within the dielectric with high density of oxygen vacancies that are induced by the effects of the electric field and temperature [17–21]. The CF formation/rupture dynamics leads to the device resistive switching (RS) operation.

The first CF formation (named forming) requires a larger bias compared to later set processes (a CF restoration after a previous reset process, where the CF is broken). The stochastic movement of oxygen

* Corresponding author.
E-mail address: jroldan@ugr.es (J.B. Roldán).

https://doi.org/10.1016/j.mssp.2025.109668
Received 17 March 2025; Received in revised form 23 April 2025; Accepted 9 May 2025
Available online 15 May 2025

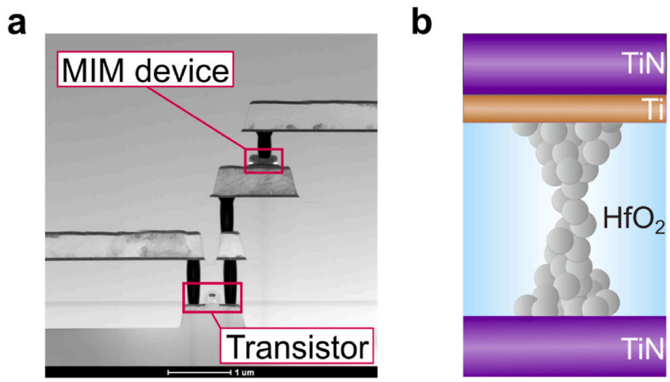

Fig. 1. **a** Cross-sectional TEM explained image of the 1T1R structure integrated within the crossbar array. **b** Schematic representation of the layered MIM stack of the measured devices and the CF responsible for the RS mechanism.

ions and the oxygen vacancies generation processes lead to the creation of ohmic percolation-paths (the CFs) that produce the inherent random behavior of resistive switching operation [22–25]. This device dynamics produces two different non-volatile conduction states (a high-resistance state (HRS) after reset processes and a low-resistance state (LRS) after set processes). Nevertheless, intermediate conduction states can also be obtained using different algorithms to improve the device performance for memory applications. In this context, further development of these devices faces two reliability hurdles: variability [23,26] and post-programming instabilities [27–30]. The second issue is essential; hence, more work needs to be done to shed light on it. For instance, the conductance drift in VCMs has been analyzed at high temperature from the experimental [28,29,31] and simulation perspectives [18,21,30,32]. Nevertheless, an in-depth statistical study that helps to advance in modeling is still lacking. We present it here. We comprehensively analyze the VCMs conductance drift and obtain the probability distribution (PD) that better fits the measurements to disentangle the experimental data structure. It is well-known that PDs help to better understand the internal performance of systems and their main physical properties [33] (a PD is a mathematical model to describe the distribution of an experiment outcome). In addition, we have employed the analysis of variance to assess the differences between the means of electrical characteristic groups; in this study, "group" refers to a collection of electrical characteristics with common features: e.g. conductance level or drift time. This study might reveal whether the observed differences are random or they reflect meaningful differences. This statistical technique has been recently applied previously in the context of resistive memories in Ref. [34].

Once the statistical characterization is performed on the experimental current data, we analyze how to introduce this variability in the Stanford model (SM) for resistive memories [35–37]. In this respect, it is essential to account for the statistical coherence in variability modeling to accurately obtain the probability distributions extracted in the current measurements. The rest of the paper is structured as follows: the fabrication and measurement setup are explained in section 2, the main results are included in section 3, a discussion linked to modeling issues is given in section 4 and the conclusions are drawn in section 5.

2. Device fabrication and experimental set-up

The fabrication of the $TiN/HfO_2/Ti/TiN$ Metal-Insulator-Metal (MIM) devices was carried out using the capabilities at IHP's pilot line, as detailed in prior publications [29,38]. The device structure, whose area is 600×600 nm^2 (see Fig. 1), is integrated on top of the

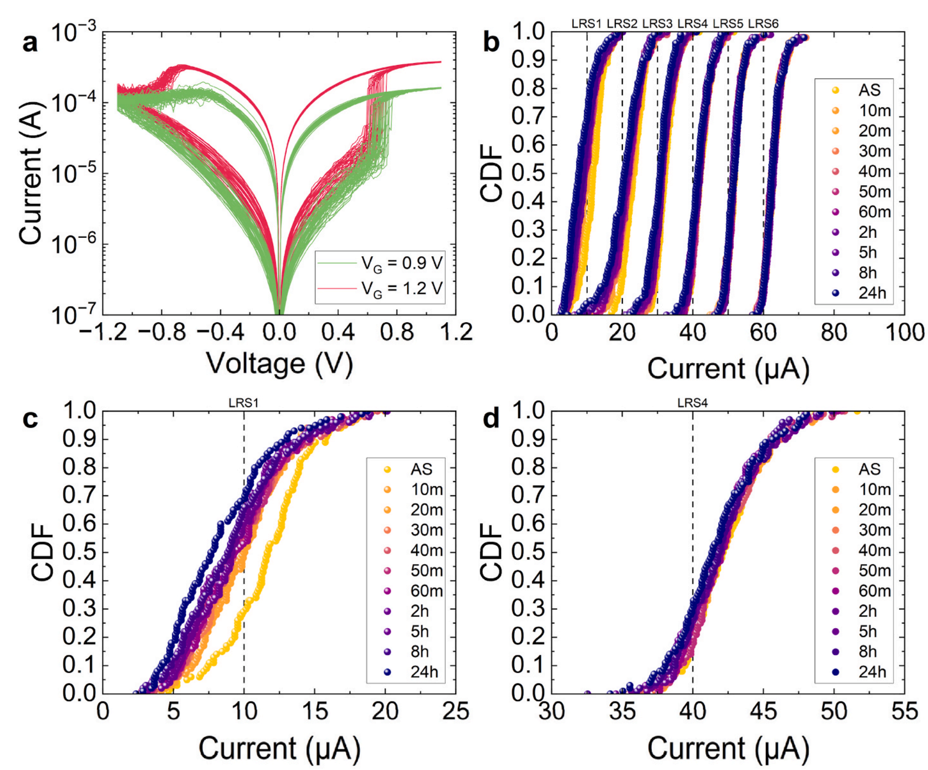

Fig. 2. **a** Current-voltage DC characteristics recorded for two distinct I_{cc} values, adjusted by modulating the transistor V_G, **b** CDFs of the read-out currents measured across 128 individual 1T1R devices for six programmed LRSs. Data were collected at eleven-time intervals: immediately after switching (AS), 10 min, 20 min, 30 min, 40 min, 50 min, 1 h, 2 h, 5 h, 8 h, and 24 h **c** (**d**) CDFs corresponding to LRS1 (LRS4), targeting a read-out current of 10 (40) μA.

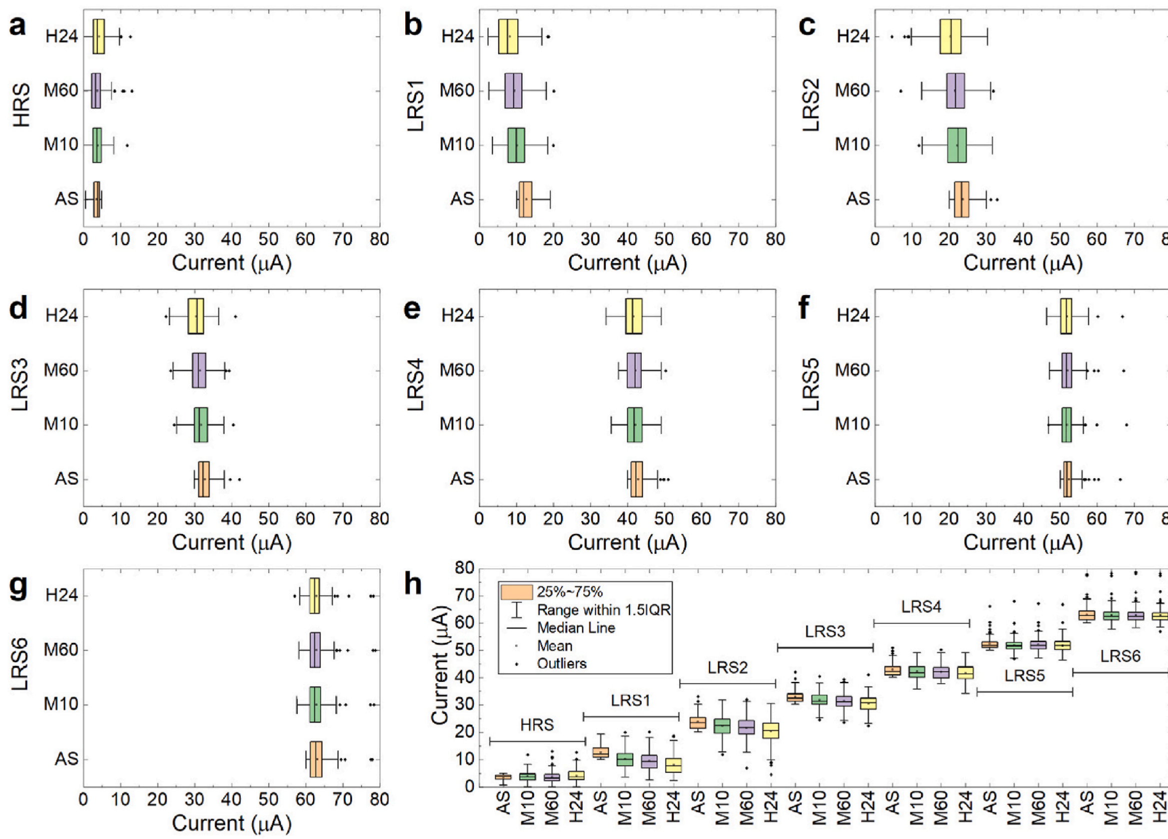

Fig. 3. **a** (**b, c, d, e, f, g**) Box plots of the experimental current distributions for the HRS (LRS1, LRS2, LRS3, LRS4, LRS5, LRS6) levels and for the post-programming times selected, namely, AS, M10, M60, and H24. **h** Box plot for all the current levels and post-programming times under consideration.

metal 2 layer of the Back-End-of-Line (BEOL) of a 130 nm CMOS technology. The bottom electrode (BE) and top electrode (TE), both made of 150 nm titanium nitride (TiN), as well as a 7 nm titanium (Ti) scavenging layer, were deposited using magnetron sputtering. A 5 nm layer of hafnium oxide (HfO_2) was deposited on the BE through Atomic Layer Deposition (ALD), ensuring excellent thickness uniformity and material quality (see Fig. 1b).

The experimental setup utilizes a 4k crossbar array of one-transistor-one-resistor (1T1R) cells. Each cell combines a 130 nm nMOS transistor in series with the MIM VCM device, as shown in Fig. 1a. This configuration enables fine current control during set and reset processes, resulting in more accurately programmed resistive states.

To prepare the devices, an initial forming process is conducted using the Incremental Step Pulse Program and Verify Algorithm (ISPVA) [39]. The voltage applied to the top electrode is gradually increased in steps of 10 mV, starting at 2.0 V and reaching up to 3.5 V, while the nMOS gate voltage (V_G) is held at 1.35 V. After forming, the reset step is performed to change the cell resistance into the HRS and stabilize the conductive filament [40]. This involves applying a V_G value of 2.3 V and progressively increasing the source voltage from 0.5 V to 2.0 V in 100 mV increments.

Regarding the multilevel cell (MLC) programming, the ISPVA technique is again used. Voltage sweeps from 0.5 V to 2.0 V in 100 mV steps are applied to the top electrode, followed by a read-out operation using a 0.2 V pulse. By adjusting V_G, six distinct conductance levels are programmed, corresponding to LRS ranging from 10 μA to 60 μA in evenly spaced intervals. Fig. 2a shows the DC current-voltage (I-V) characteristics measured for two separate groups, each consisting of 50 reset-set cycles. The distinction between the groups lies in the value of I_{cc}, which was controlled by adjusting V_G. This approach highlights the feasibility of MLC operation and the good device reliability with relatively low cycle-to-cycle variability.

In Fig. 2b, the experimental read-out current cumulative distribution functions (CDFs) are presented for six programmed resistance levels in a sample set of 128 individual 1T1R devices within the crossbar array. Data were collected at eleven distinct time intervals: immediately after switching (AS), 10 min, 20 min, 30 min, 40 min, 50 min, 1 h, 2 h, 5 h, 8 h, and 24 h. These measurements capture the temporal evolution of the device electrical characteristics. The six LRSs were programmed to target specific read-out current levels: 10 μA for LRS1, 20 μA for LRS2, 30 μA for LRS3, 40 μA for LRS4, 50 μA for LRS5, and 60 μA for LRS6. For the sake of clarity Fig. 2c specifically illustrates the results for LRS1, which corresponds to the lowest programmed current level of 10 μA, while Fig. 2d focuses on LRS4, representing an intermediate level of 40 μA. All the electrical measurements were carried out at room temperature (300K) in a controlled laboratory environment, and the devices were not subjected to thermal stress.

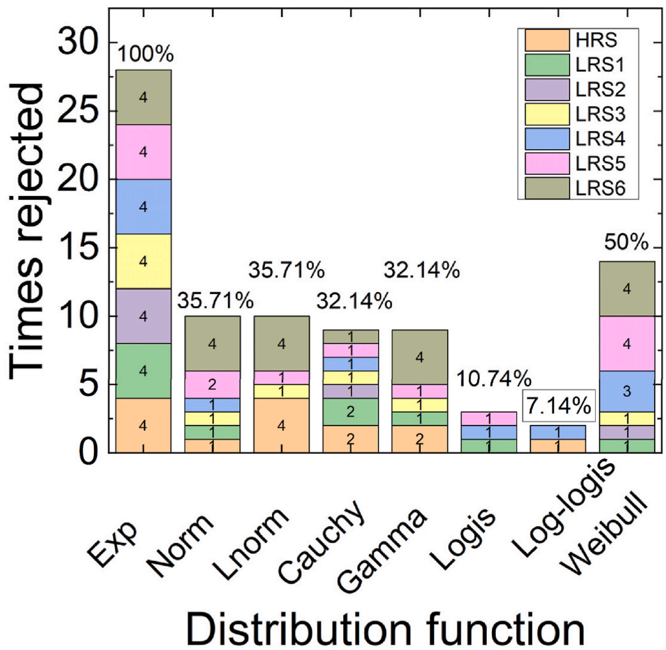

Fig. 4. Number of times a PD does not fit well the current distributions regarding conductance levels (6 levels) and post-programming times (4 times) under consideration (see Supplementary Table S1). The total number of unsuccessful fits per PD for the four times under consideration is shown (the color code identifies the results for each current level). The numbers above the columns show the relative proportion of unsuccessful fits for each PD, accounting for all the current levels and times under consideration. (For interpretation of the references to color in this figure legend, the reader is referred to the Web version of this article.)

3. Results

For the reliability analysis, we have performed the procedures needed to identify the PD that better describes the temporal evolution of the experimental current distributions (we consider different classical PDs: Exponential, Normal, Log-normal, Cauchi, Gamma, Logistic, Log-logistic, Weibull). We take into account the measurements after switching (AS), after 10 min (m10), after 60 min (m60), and after 24 h (h24). See in Fig. 3 the box plots of the data we have employed in our analysis.

Firstly, we estimate the PD parameters for each dataset (that is, the current data in the four post-programming times aforementioned for each current level) by the maximum likelihood method [41]. After this, we go through the Kolmogorov-Smirnov's test. This statistical procedure compares the experimental CDF and the estimated one to check if the experimental data reasonably follows the proposed distribution [42]. Fig. 4 displays the number of times each PD was rejected (does not fit correctly the experimental data) for a significance level of $\alpha = 0.05$.

The log-logistic PD (see Supplementary note 1) is the best choice for our data (only a 7.14 % of rejection is achieved). In fact, with $\alpha = 0.01$, a 0 % would be reached. We have fitted the experimental data with this function for the scale and shape parameters obtained, see Fig. 5.

We have also detailed the estimations achieved in each scenario above including the p-value associated to the Kolmogorov-Smirnov's test (see Supplementary Note 2, Tables S2–S8). Notice that as the post-programming time rises the shape parameter for the log-logistic PD decreases, what is indicative of a higher variability. In contrast, the scale parameter of the log-logistic PD decreases, which means a reduction of the device current (see Fig. 6).

Analyzing the data for the different conductance levels, we observe a scale parameter shift (related to the median current) to lower current values. In addition, a reduction of the shape parameter is observed as the conductance level decreases, indicating increased variability. We observe that the conductance levels corresponding to LRS1, LRS2, and LRS3 exhibit a higher dispersion in the measured current values, as evidenced by the broader interquartile ranges and whiskers in the box plots (Fig. 3). This behavior is linked to the formation of thinner and less compact CFs at these lower current levels. In such cases, a small random rearrangement of oxygen vacancies during a post-programming drift can lead to relatively large variations in the CF conductance, thus increasing the variability [18,21,30]. In this case a random variation of some oxygen vacancies, as the drift time increases, produces a greater percentage variation of the total device conductance because the CFs size and compactness rises at higher conductance levels [21,30].

As shown in Fig. 6, the log-logistic PD broadens with increasing post-programming times, which reflects the growing current variability. This broadening is captured by the decrease in the shape parameter, and it leads to an increase in the PD full width at half maximum (FWHM). The FWHM can be interpreted as a measure of statistical dispersion (see Supplementary Note 1); in our case, a wider PD implies more significant drift-related effects. This issue is more relevant in thinner CFs (lower conductance levels), where small structural changes (linked for instance to oxygen vacancies recombination) can lead to noticeable conductance changes. The CDFs for both experimental and modeled data are shown in Fig. 7.

Finally, we can determine if data have the same statistical structure in terms of the PD that describes them. Taking into consideration our assumption of the appropriateness of the log-logistic PD to model the experimental current distributions, this would mean determining significant differences in the shape and scale parameters among them. On the one hand, fixing the post-programming time, a comparison of the data linked to pairs of conductance levels would be performed: LRS1-HRS, LRS1-LRS2 … See the detailed results in the Supplementary note 3. In general, there are important differences among conductance levels when post-programming times are fixed. This fact is mainly caused by the scale parameter, linked to the conductance level. On the other hand, when we fix the conductance level, the only significant differences correspond to the AS compared to the rest of post-programming times (low p-values). In particular, for LRS6 the differences vanish. In this case the linked CFs are more compact (a higher oxygen vacancies density is found) than for lower conductance levels; therefore, random variations in time have less impact in the whole CF, which is thicker and denser [30].

We have also employed the analysis of variance technique [43] to test the effect of the temporal evolution and the conductance level over the current distribution. In particular, we apply a two-way analysis of variance with repeated measures, since the information is measured repeatedly in time (post-programming times) and classified in independent groups (conductance levels). Given that our data do not follow a normal distribution, we assume a semi-parametric approach to avoid the restrictive assumptions that requires the parametric one [44]. The results obtained are given in Table S9 in the Supplementary note 4. This study reveals significant differences in the datasets we measured for the conductance levels and post-programming times under study. Besides, interaction between both factors (conductance level and

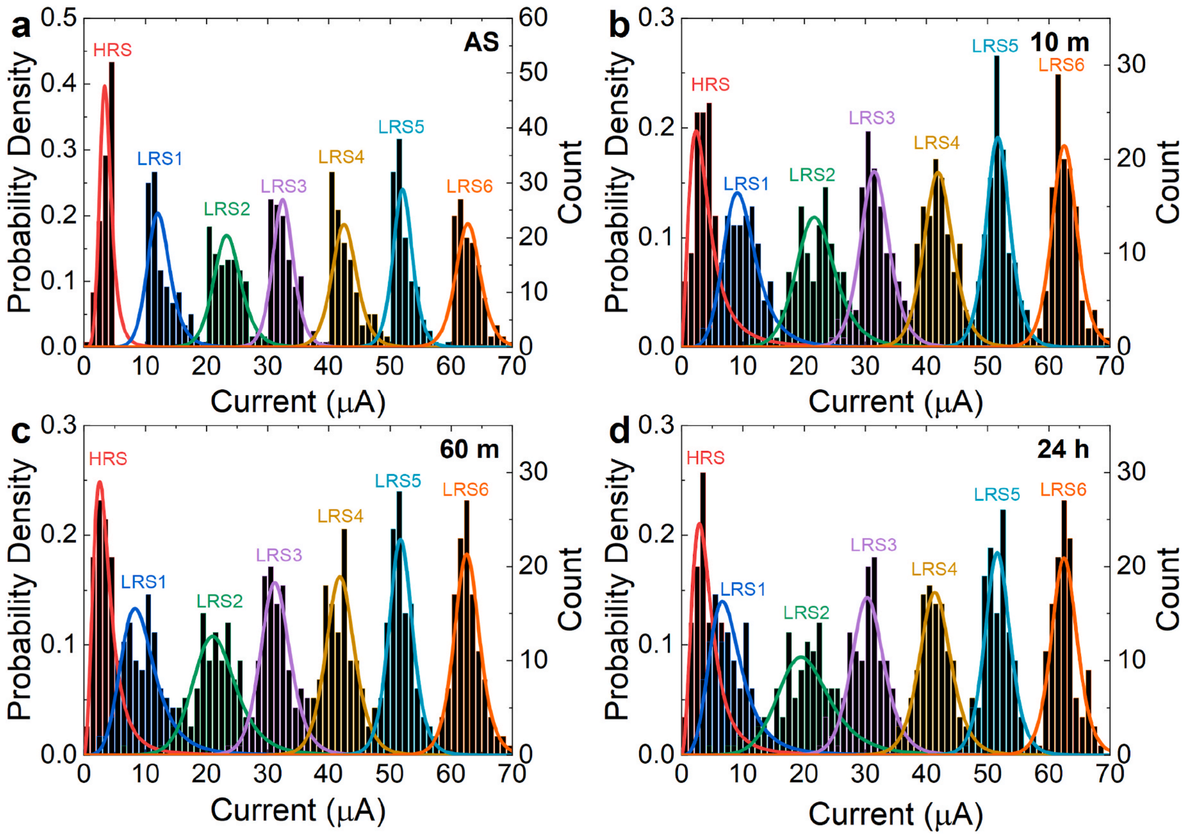

Fig. 5. a (b, c, d) Experimental and modeled current distributions for the 6 conductance levels studied. The modeling is linked to the log-logistic PD and the parameters obtained for the post-programming times (AS, 10m, 60m, 24h).

post-programming time) is found; in this respect, statistically, the effect of one factor depends on the values of the other. In our study, this fact is interpreted as the effect of the post-programming time over the current is different depending on the conductance level.

Finally, a post-hoc analysis [45] fixing the current level is made to analyze in more detail the statistical role of post-programming times. A post-hoc analysis shows if there are significant differences, on average, among post-programming times when compared one-to-one. The results obtained are given in Table S10 in the Supplementary note 4. In broad terms, only differences are detected when AS is involved in LRS1, LRS2 and LRS3, which are in concordance with the reliability study shown above. Therefore, these results might reveal that the current is stabilized as time goes by and that the post-programming time effect is lower as the conductance level increases.

4. Discussion

Once the statistical analysis of the measurements is carried out, there are several issues that can be discussed. In general, variability is modeled without considering the PD of the current values, just the magnitude of the variations is described. We have advanced in this work in describing the PD of experimental data and, in this context, we can deepen on the modeling implications. To do so, we have taken into consideration the Stanford Model [35–37]. This model, implemented for circuit simulation purposes, is based on the calculation of the CF dynamics to obtain the device current. In particular, the gap (g) (between the CF tip and the electrode) is employed as the state variable to describe the resistive switching operation [35–37], see Equation (1).

$$\frac{dg}{dt} = -v_0 e^{\frac{-E_{g,m}}{k_B T}} \sinh\left(\frac{\gamma(g) a_0 q V_{RRAM}}{t_{ox} k_B T}\right), \tag{1}$$

where t_{ox} is the dielectric layer thickness, E_g (E_m) is the activation energy (migration barrier) for vacancy generation (oxygen ion migration) in set (reset) processes, v_0 stands for the velocity containing the attempt-to-escape frequency, a_0 is the atom spacing and V_{RRAM} the device applied voltage, which drops mainly across the gap, k_B is Boltzmann's constant, T the device temperature that is obtained by solving a simplified version of the heat equation [36,37], and q stands for the electron charge. Parameter γ is the electric field local enhancement factor that takes into consideration the polarizability of the material [37] (it can be obtained as $\gamma = \gamma_0 - \omega g^{\psi}$, where γ_0, ω and ψ are fitting parameters). Set ($g \approx 0$) and reset ($g > 0$) processes switch the device resistance between the LRS and HRS.

An approach to model variability has been also implemented in SM [35,36]. It is introduced by using Equation (2) to include a random variation on the gap calculation.

$$g_{t+\Delta t} = \int \left(\frac{dg}{dt} + \delta_g \times \chi(t)\right) dt, \tag{2}$$

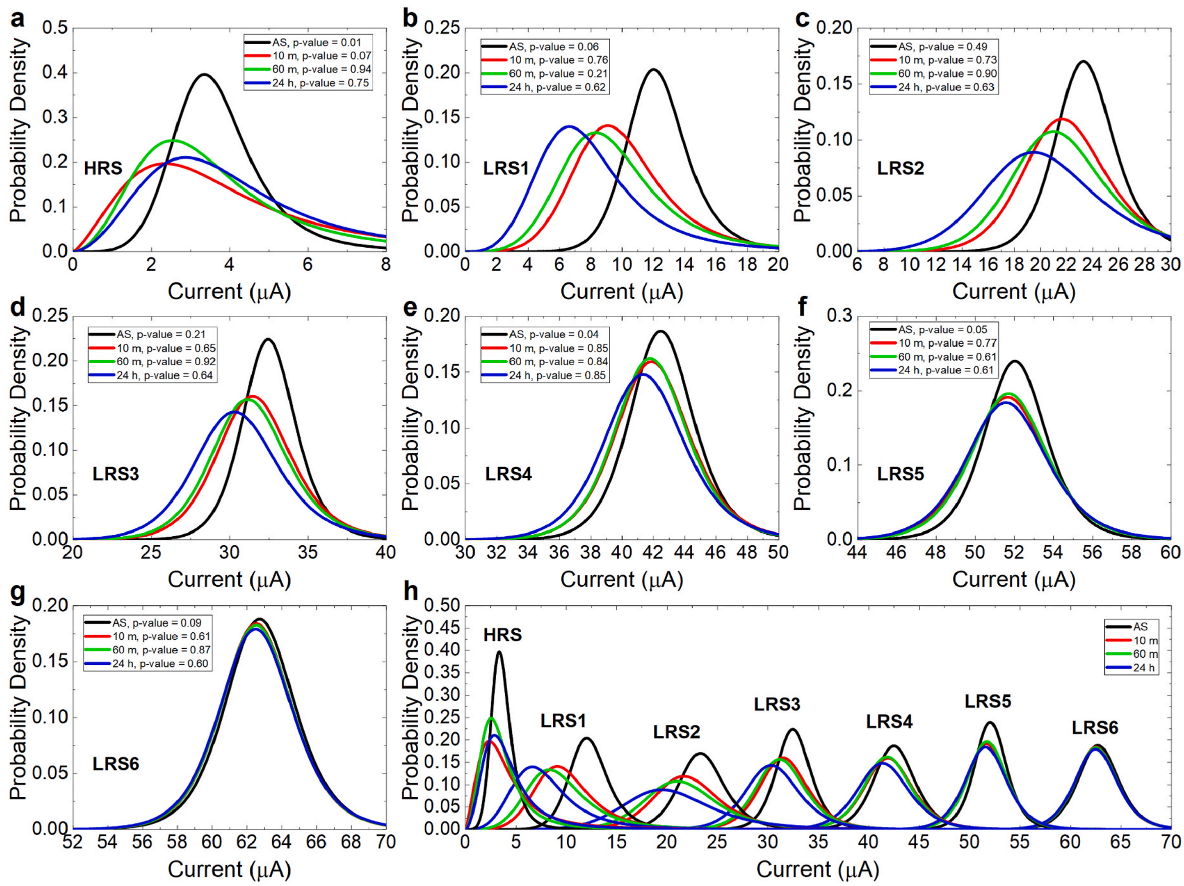

Fig. 6. **a** (**b, c, d, e, f, g**) Log-logistic probability density functions corresponding to the different conductance levels (LRS1, LRS2, LRS3, LRS4, LRS5, LRS6), using the fitting parameters obtained in Tables S2–S8 in the Supplementary Information. **h** Log-logistic probability density functions corresponding to all the conductance levels.

where δ_g is the strength of the random variations and $\chi(t)$ stands for the PD. In the original version of SM, a zero-mean Gaussian distributed sequence with a unity standard deviation is proposed [37], which is randomly generated at each time step (Equation (2)). Nevertheless, it comes up at this point the consideration of the appropriateness of a Gaussian PD, taking into account that different RRAM technologies could lead to different current PDs. In this respect, in our devices we obtained the log-logistic PD. Therefore, from the modeling perspective, for our technology we need to assess the PD to be used in Equation (2) to obtain a current log-logistic PD, assuming that for SM the current is obtained in Equation (3) [37].

$$I(g, V_{RRAM}) = I_0 \, e^{\frac{-g}{g_0}} \sinh\left(\frac{V_{RRAM}}{V_0}\right), \tag{3}$$

where I_0, g_0 and V_0 are fitting parameters.

Since an exponential function links the current with g in Equation (3), it is clear that we could obtain a log-logistic PD for the current in a variability analysis (see Supplementary note 5). In a different way, if a logistic PD were considered for $\chi(t)$ in Equation (2) (i.e. the randomness is included in the iterative process for g calculation), a non-logistic PD would be obtained for g, because the sum of logistic distributions is not a logistic PD. Consequently, a calculation for g without variability is needed in the iterative process, and the noise is added after the g dynamics is solved. That would mean the g calculation without the extra noise, and later on, at each time step, a random number following the logistic PD should be added weighted by δ_g. However, the noise is not taken into consideration in the new g calculation, for the next time step, to avoid producing a non-logistic PD.

5. Conclusions

We have conducted an extensive statistical study of conductance drift in HfO_2-based RRAM devices. By analyzing the conductance evolution over multiple drift times and for different current levels, we demonstrated that the log-logistic probability distribution provides the most accurate representation of measured data. This result is particularly significant as it allows a precise device variability characterization, which is essential for improving reliability in both non-volatile memory and neuromorphic applications. A further variability study based on the analysis of variance technique confirms that the statistical effects of the drift time on the current depend on the current level. The implications of our statistical study are extended in the compact modeling arena. A new proposed technique for variability implementation in the Stanford

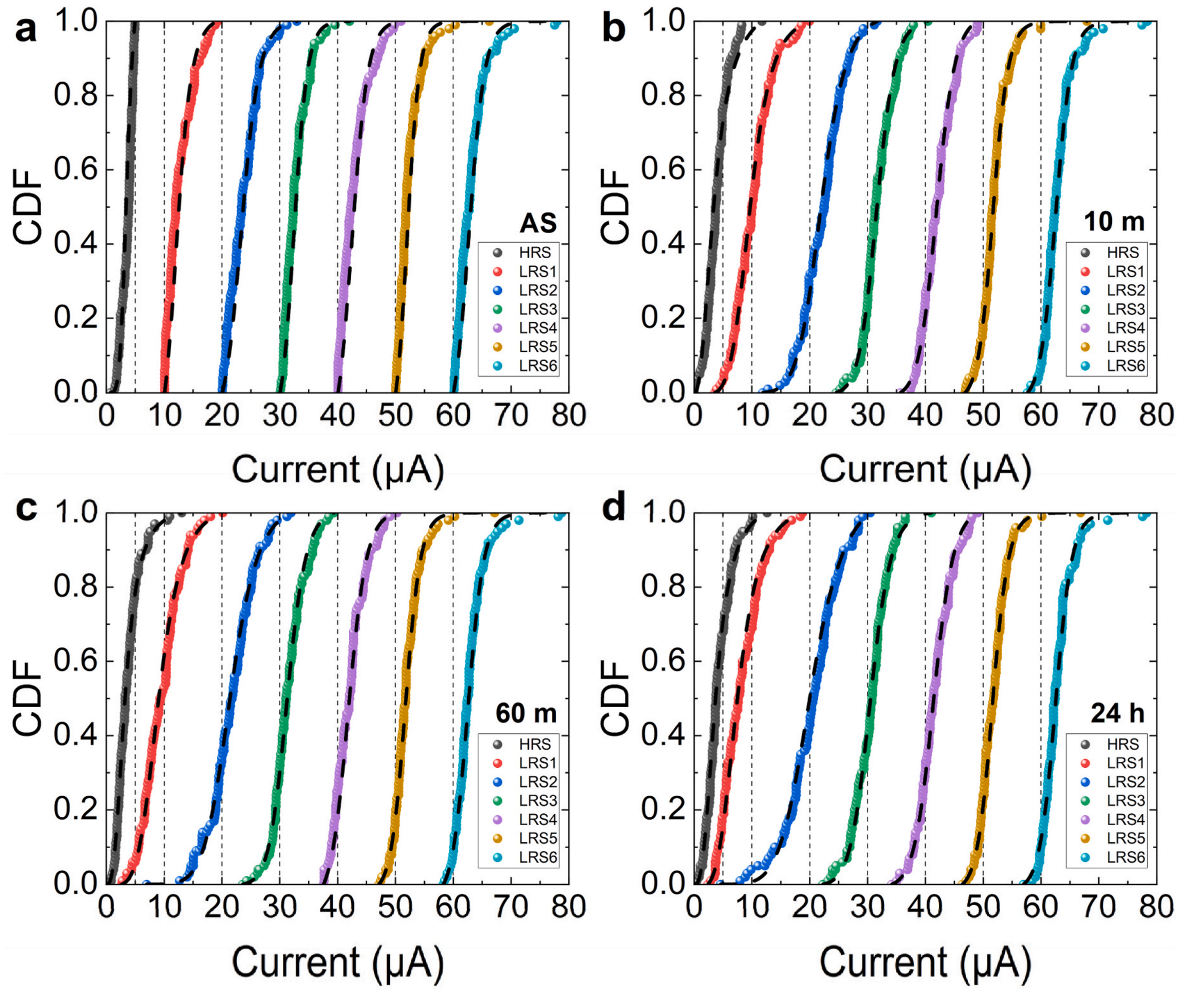

Fig. 7. **a (b, c, d)** CDFs of experimental (symbols) and model (dashed) current data for the multi-levels under consideration. The modeling corresponds to the log-logistic PD and the parameters obtained for the AS (10 m, 60m, 24h) post-programming times.

model state variable can produce the measured current probability distributions.

CRediT authorship contribution statement

D. Maldonado: Visualization, Investigation, Formal analysis, Data curation. **C. Acal:** Writing – review & editing, Writing – original draft, Investigation, Formal analysis, Data curation. **H. Ortiz:** Investigation, Formal analysis, Data curation. **A.M. Aguilera:** Writing – review & editing, Investigation, Funding acquisition. **J.E. Ruiz-Castro:** Writing – review & editing, Validation, Investigation. **A. Cantudo:** Software, Investigation. **A. Baroni:** Investigation, Data curation. **K. Dorai Swamy Reddy:** Investigation. **S. Pechmann:** Investigation. **M. Uhlmann:** Investigation. **C. Wenger:** Writing – review & editing, Resources, Project administration, Conceptualization. **E. Pérez:** Writing – review & editing, Writing – original draft, Project administration, Investigation, Funding acquisition, Conceptualization. **J.B. Roldán:** Writing – review & editing, Writing – original draft, Project administration, Funding acquisition, Conceptualization.

Declaration of competing interest

The authors declare that they have no known competing financial interests or personal relationships that could have appeared to influence the work reported in this paper.

Acknowledgements

The authors thank the support of the German Research Foundation (DFG) for funding this work under grant 546680029. They also acknowledge project PID2022-139586NB-C44 and PID2023-149087NB-I00 funded by MCIN/AEI/10.13039/501100011033 and FEDER, EU and the "María de Maeztu" Excellence Unit IMAG reference CEX2020-001105-M, funded by MCIN/AEI/10.13039/501100011033.

Appendix A. Supplementary data

Supplementary data to this article can be found online at https://doi.org/10.1016/j.mssp.2025.109668.

Data availability

Data will be made available on request.

References

[1] Mario Lanza, Abu Sebastian, Wei D. Lu, Manuel Le Gallo, Meng-Fan Chang, Deji Akinwande, Francesco M. Puglisi, Husam N. Alshareef, Ming Liu, Juan B. Roldan, Memristive technologies for data storage, computation, encryption and radio-frequency communication, Science 376 (6597) (2022) 1–13, eabj9979.

[2] M. Salinga, B. Kersting, I. Ronneberger, V.P. Jonnalagadda, X.T. Vu, M. Le Gallo, I. Giannopoulos, O. Cojocaru-Mirédin, R. Mazzarello, A. Sebastian, Monatomic phase change memory, Nat. Mater. 17 (2018) 681–685.

[3] A.V. Khvalkovskiy, D. Apalkov, S. Watts, R. Chepulskii, R.S. Beach, A. Ong, et al., Basic principles of STT-MRAM cell operation in memory arrays, J. Phys. D Appl. Phys. 46 (2013) 139601.

[4] M. Trentzsch, et al., A 28nm HKMG super low power embedded NVM technology based on ferroelectric FETs. 2016 IEEE International Electron Devices Meeting (IEDM), 2016, pp. 11.5.1–11.5.4.

[5] C.-C. Chou, et al., A 22nm 96KX144 RRAM macro with a self-tracking reference and a low ripple charge pump to achieve a configurable read window and a wide operating voltage range, in: 2020 IEEE Symposium on VLSI Circuits, 2020, pp. 1–2. Honolulu, HI, USA.

[6] P. Jain, et al., A 3.6 Mb 10.1 Mb/mm2 embedded non-volatile Re-RAM macro in 22nm FinFET technology with adaptive forming/set/reset schemes yielding down to 0.5 V with sensing time of 5ns at 0.7 V. 2019 IEEE International Solid-State Circuits Conference - (ISSCC), 2019, pp. 212–214. San Francisco, CA, USA.

[7] N. Wainstein, G. Adam, E. Yalon, S. Kvatinsky, Radiofrequency switches based on emerging resistive memory technologies-a survey, Proc. IEEE 109 (1) (2020) 77–95.

[8] Z. Wei, et al., True random number generator using current difference based on a fractional stochastic model in 40-nm embedded ReRAM, in: 2016 IEEE International Electron Devices Meeting (IEDM), 2016, pp. 4.8.1–4.8.4. San Francisco, CA.

[9] R. Romero-Zaliz, A. Cantudo, E. Pérez, F. Jiménez-Molinos, C. Wenger, J.B. Roldán, An analysis on the architecture and the size of quantized hardware neural networks based on memristors, Electronics 10 (2021) 3141.

[10] S.-i. Yi, J.D. Kendall, R.S. Williams, S. Kumar, Activity-Difference training of deep neural networks using memristor crossbars, Nat. Electron. 6 (2022) 45–51.

[11] W. Zhang, et al., Edge learning using A fully integrated neuro-inspired memristor chip, Science 381 (2023) 1205–1211.

[12] W. Song, et al., Programming memristor arrays with arbitrarily high precision for analog computing, Science 383 (2024) 903–910.

[13] F. Aguirre, A. Sebastian, M. le Gallo, W. Song, T. Wang, J. Joshua Yang, W. Lu, M.-F. Chang, D. Ielmini, Y. Yang, A. Mehonic, A. Kenyon, M. Villena, J. Roldan, Y. Wu, H.-H. Hsu, N. Raghavan, J. Suñé, E. Miranda, A. Eltawil, G. Setti, K. Smagulova, K. Salama, O. Krestinskaya, X. Yan, K. Ang, S. Jain, S. Li, O. Alharbi, S. Pazos, M. Lanza, Hardware implementation of memristor-based artificial neural networks, Nat. Commun. 15 (2024) 1974.

[14] D. Maldonado, A. Cantudo, D.V. Guseinov, M.N. Koryazhkina, E.V. Okulich, D. I. Tetelbaum, N.O. Bartev, N.G. Danchenko, V.A. Pikar, A.V. Teterevkov, F. Jiménez-Molinos, A.N. Mikhaylov, J.B. Roldán, A statistical and modeling study on the effects of radiation on Au/Ta/ZrO2(Y)/Pt/Ti memristive devices, Chaos Solitons Fractals 191 (2025) 115909.

[15] D.J. Wouters, S. Menzel, J.A.J. Rupp, T. Hennen, R. Waser, On the universality of the I–V switching characteristics in non-volatile and volatile resistive switching oxides. Faraday Discussions, The Royal Society of Chemistry, 2019, pp. 1359–6640.

[16] C. Funck, S. Menzel, Comprehensive model of electron conduction in oxide-based memristive devices, ACS Appl. Electron. Mater. 3 (2021) 3674–3692.

[17] A. Padovani, L. Larcher, O. Pirrotta, L. Vandelli, G. Bersuker, Microscopic modeling of HfOx RRAM operations: from forming to switching, IEEE Trans. Electron. Dev. 62 (6) (June 2015) 1998–2006, https://doi.org/10.1109/TED.2015.2418114.

[18] S. Aldana, P. García-Fernández, R. Romero-Zaliz, M.B. González, F. Jiménez-Molinos, F. Gómez-Campos, F. Campabadal, J.B. Roldán, Resistive Switching in HfO2 based valence change memories, a comprehensive 3D kinetic Monte Carlo approach, J. Phys. Appl. Phys. 53 (2020) 225106.

[19] G. Bersuker, D.C. Gilmer, D. Veksler, P. Kirsch, L. Vandelli, A. Padovani, L. Larcher, K. McKenna, A. Shluger, V. Iglesias, M. Porti, M. Nafría, Metal oxide resistive memory switching mechanism based on conductive filament properties, J. Appl. Phys. 110 (2011) 124518.

[20] L. Larcher, A. Padovani, L. Vandelli, A simulation framework for modeling charge transport and degradation in high-k stacks, J. Comput. Electron. 12 (4) (2013) 658–665.

[21] S. Aldana, E. Pérez, F. Jimenez-Molinos, C. Wenger, J.B. Roldán, Kinetic Monte Carlo analysis of data retention in Al:HfO_2-based resistive random access memories, Semicond. Sci. Technol. 35 (2020) 115012.

[22] D. Ielmini, R. Waser, Resistive Switching: from Fundamentals of Nanoionic Redox Processes to Memristive Device Applications, Wiley-VCH, 2015.

[23] J.B. Roldán, E. Miranda, D. Maldonado, A.N. Mikhaylov, N.V. Agudov, A. A. Dubkov, M.N. Koryazhkina, M.B. González, M.A. Villena, S. Poblador, M. Saludes-Tapia, R. Picos, F. Jiménez-Molinos, S.G. Stavrinides, E. Salvador, F. J. Alonso, F. Campabadal, B. Spagnolo, M. Lanza, L.O. Chua, Variability in resistive memories, Advan. Intellig. Syst. (2023) 2200338.

[24] S. Dirkmann, J. Kaiser, C. Wenger, T. Mussenbrock, Filament growth and resistive switching in hafnium oxide memristive devices, ACS Appl. Mater. Interfaces 10 (17) (2018) 14857–14868.

[25] C. Acal, D. Maldonado, A.M. Aguilera, K. Zhu, M. Lanza, J.B. Roldán, Holistic variability analysis in resistive switching memories using a two-dimensional variability coefficient, ACS Appl. Mater. Interfaces 15 (15) (2023) 19102–19110.

[26] E. Pérez, D. Maldonado, C. Acal, J.E. Ruiz-Castro, F.J. Alonso, A.M. Aguilera, F. Jiménez-Molinos, Ch Wenger, J.B. Roldán, Analysis of the statistics of device-to-device and cycle-to-cycle variability in TiN/Ti/Al:HfO_2/TiN RRAMs, Microelectron. Eng. 214 (2019) 104–109.

[27] A. Fantini, G. Gorine, R. Degraeve, L. Goux, C.Y. Chen, A. Redolfi, S. Clima, A. Cabrini, G. Torelli, M. Jurczak, Intrinsic Program Instability in HfO_2 RRAM and consequences on program algorithms, in: 2014 IEEE International Electron Devices Meeting, 2015, pp. 7.5.1–7.5.4.

[28] E. Pérez, C. Zambelli, M. Kalishettyhalli Mahadevaiah, P. Olivo, C. Wenger, Toward reliable multi-level operation in RRAM arrays: improving post-algorithm stability and assessing endurance/data retention, J. Electron Dev. Soc. 7 (2019) 740–747.

[29] A. Baroni, A. Glukhov, E. Pérez, C. Wenger, D. Ielmini, P. Olivo, C. Zambelli, Low conductance state drift characterization and mitigation in resistive switching memories (RRAM) for artificial neural networks, IEEE Trans. Device Mater. Reliab. 22 (3) (2022) 340–347.

[30] D. Maldonado, A. Baroni, S. Aldana, K.D.S. Reddy, S. Pechmann, C. Wenger, J. B. Roldan, E. Perez, Kinetic Monte Carlo simulation analysis of the conductance drift in Multilevel HfO2-based RRAM devices, Nanoscale 16 (2024) 19021–19033.

[31] B. Traoré, P. Blaise, E. Vianello, H. Grampeix, S. Jeannot, L. Perniola, Y. Nishi, On the origin of low-resistance state retention failure in HfO 2-based RRAM and impact of doping/alloying, IEEE Trans. Electron. Dev. 62 (12) (2015) 4029–4036.

[32] N. Raghavan, D.D. Frey, M. Bosman, K.L. Pey, Statistics of retention failure in the low resistance state for hafnium oxide RRAM using a Kinetic Monte Carlo approach, Microelectron. Reliab. 55 (9–10) (2015) 1422–1426.

[33] J.E. Ruiz-Castro, C. Acal, J.B. Roldán, An approach to non-homogenous phase-type distributions through multiple cut-points, Qual. Eng. 35 (4) (2023) 619–638.

[34] A.M. Aguilera, C. Acal, M.C. Aguilera-Morillo, F. Jiménez-Molinos, J.B. Roldán, Homogeneity problem for basis expansion of functional data with applications to resistive memories, Math. Comput. Simulat. 186 (2021) 41–51.

[35] P. Chen, S. Yu, Compact modeling of RRAM devices and its applications in 1T1R and 1S1R array design, IEEE Trans. Electron. Dev. 62 (12) (Dec. 2015) 4022–4028.

[36] X. Guan, S. Yu, H.-S. Philip Wong, A SPICE compact model of metal oxide resistive switching memory with variations, Electron Device Lett. IEEE 33 (10) (Oct. 2012) 1405–1407.

[37] Z. Jiang, Y. Wu, S. Yu, Member, L. Yang, K. Song, Z. Karim, H.-S.P. Wong, A compact model for metal–oxide resistive random access memory with experiment verification, IEEE Trans. Electron. Dev. 63 (May 2016) 1884–1892.

[38] M.K. Mahadevaiah, M. Lisker, M. Fraschke, S. Marschmeyer, D. Schmidt, Ch Wenger, E. Perez, A. Mai, Optimized HfO_2-based MIM module fabrication for emerging memory applications, in: Proceedings of the 235th ECS Meeting, vol. 92, 2019, pp. 211–221.

[39] F. Crupi, F. Filice, A. Grossi, P. Olivo, E. Perez, C. Wenger, Implications of the incremental Pulse and verify algorithm on the forming and switching distributions in RERAM arrays, IEEE Trans. Device Mater. Reliab. 16 (2016) 413–418.

[40] E. Pérez, Mahadevaiah, M.K. Zambelli, P. Olivo, C. Wenger, Data retention investigation in Al: HfO2-based resistive random access memory arrays by using high-temperature accelerated tests, J. Vac. Sci. Technol. B 37 (1) (2019).

[41] W.N. Venables, B.D. Ripley, Modern Applied Statistics with S, fourth ed., Springer, 2002.

[42] V.W. Berger, Y. Zhou, in: N. Balakrishnan, T. Colton, B. Everitt, W. Piegorsch, F. Ruggeri, J.L. Teugels (Eds.), Kolmogorov–Smirnov Test: Overview, Wiley StatsRef: Statistics Reference Online, 2014.

[43] H. Scheffe, The Analysis of Variance, vol. 72, John Wiley & Sons, 1999.

[44] S. Friedrich, F. Konietschke, M. Pauly, Resampling-based analysis of multivariate data and repeated measures designs with the R package MANOVA.RM, The R Journal 11 (2) (2019) 380–400.

[45] D.G. Pereira, A. Afonso, F.M. Medeiros, Overview of Friedman's test and post-hoc analysis, Commun. Stat. Simulat. Comput. 44 (10) (2015) 2636–2653.